

# Journal of Materials Chemistry B

Accepted Manuscript



This is an *Accepted Manuscript*, which has been through the Royal Society of Chemistry peer review process and has been accepted for publication.

*Accepted Manuscripts* are published online shortly after acceptance, before technical editing, formatting and proof reading. Using this free service, authors can make their results available to the community, in citable form, before we publish the edited article. We will replace this *Accepted Manuscript* with the edited and formatted *Advance Article* as soon as it is available.

You can find more information about *Accepted Manuscripts* in the [Information for Authors](#).

Please note that technical editing may introduce minor changes to the text and/or graphics, which may alter content. The journal's standard [Terms & Conditions](#) and the [Ethical guidelines](#) still apply. In no event shall the Royal Society of Chemistry be held responsible for any errors or omissions in this *Accepted Manuscript* or any consequences arising from the use of any information it contains.

---

1 **Full paper**

2

3 **Effectively promote wound healing of cellulose/gelatin sponges**  
4 **constructed directly from cellulose solution**

5 Ying Pei<sup>1δ</sup>, Dongdong Ye<sup>1δ</sup>, Qi Zhao<sup>2</sup>, Xueying Wang<sup>1</sup>, Chun Zhang<sup>2</sup>,

6 Weihua Huang<sup>1</sup>, Nu Zhang<sup>2</sup>, Shiqing Liu<sup>2</sup>, Lina Zhang<sup>1\*</sup>

7

8 1. College of Chemistry & Molecule Sciences, Wuhan University,  
9 Wuhan 430072, P. R. China

10 2. Renmin Hospital, Wuhan University, Wuhan 430072, P. R. China

11 δ . These authors contributed equally to this paper

12 \* . The corresponding author, Fax: +86-27-68754067; Tel: +86-27-87219274;

13 E-mail: zhangln@whu.edu.cn

14

---

15 **Abstract:** Wound dressing is of critical importance for wound repair, and the  
16 traditional cotton gauze derived from cellulose has commonly been used in clinical  
17 practice for a long time. However, cotton gauze does not possess active healing ability.  
18 To search new wound dressings, in this work, cellulose sponge was fabricated directly  
19 from the cellulose solution in the NaOH/urea aqueous system with cooling, and then  
20 the cellulose/gelatin composite sponges were constructed successfully via a green and  
21 cost-effective pathway. The structure and physical properties of the sponges were  
22 characterized, and their cytocompatibility and *in vivo* wound healing were evaluated.  
23 The results indicated that, compared with cotton gauze, the cellulose sponge  
24 effectively promoted wound healing, as a result of the presence of the macro- and  
25 micro porous architecture. Furthermore, the gelatin and basic fibroblast growth factor  
26 (bFGF) were immobilized in the cellulose sponge through hydrogen bonding to retain  
27 their inherent biocompatibility, leading to the excellent repairing efficacy. Especially,  
28 for full-thickness coetaneous wound model, the complete wound healing time for the  
29 wounds treated with bFGF-loaded cellulose sponges was 7 days faster than that  
30 treated with gauze. The pores with thin wall in the cellulose composite sponges  
31 played an important role in achieving the highly effective wound healing, which could  
32 fit the requirements of oxygen permeability, controlled water vapor evaporation and  
33 wound exudates absorption.

34 **Keywords:** Cellulose sponge, wound dressing, porous architecture, gelatin, wound  
35 repairing efficacy.

36

---

## 37 1. Introduction

38 Skin, as the largest organ in the body, plays an important role in protection against  
39 invasion from the environment. On a global scale, about 234.2 million people undergo  
40 surgical procedures because of accident or healthy problems, resulting in huge  
41 demand for skin wound dressings<sup>1</sup>. Constructing effective dressing is essential for  
42 promoting wound healing in view of the health care issues. Basically, a desirable  
43 wound dressing should possess gas permeability and biocompatibility. It should keep  
44 moist at the injury interface as well as acting as a barrier to microorganisms<sup>2</sup>.  
45 Recently, natural<sup>3</sup>, synthetic<sup>4</sup>, and hybrid organic materials<sup>5</sup> have been employed to  
46 construct wound dressings. Synergistic compositions and novel structural design  
47 endow these dressings with functionality such as antimicrobial properties<sup>6</sup>, growth  
48 factors<sup>7</sup> or drug release abilities<sup>8</sup>, and biodegradable properties<sup>9</sup>, thus helping to  
49 hasten up the healing process. Especially, the dressings were mostly designed to  
50 porous structure, benefiting to fit the requirements of gas permeability, controlled  
51 water vapor evaporation and wound exudates absorption. It is worth noting that  
52 natural polymers such as gelatin<sup>10</sup>, collagen<sup>11</sup>, silk fibroin<sup>12</sup>, cellulose<sup>13</sup>, alginate<sup>14</sup>,  
53 chitosan, and chitin<sup>2</sup> have become good candidates for the fabrication of wound  
54 dressing due to their non-cytotoxicity and hydrophilicity. Cellulose is the most  
55 abundant renewable natural polymer, and it, as well as its derivatives, have been  
56 widely used for biological and medical application including scaffold<sup>15,16</sup>, medical  
57 system development<sup>17</sup>, drug diagnosis<sup>18</sup> and orthopedic biomaterial<sup>19</sup>, showing good  
58 biocompatibility by *in vitro* and *in vivo* tests<sup>20,21</sup>. Though the traditional cellulose

---

59 gauze based dressing has commonly been used in clinical practice for a long time, it  
60 does not possess active healing capabilities, limited by its low efficiency to absorb the  
61 exudates and to prevent bacteria from growth and migration. Thus, searching for new  
62 wound dressing based on cellulose is essential for the effectively promote wound  
63 healing. Recently, bacterial cellulose with nanofiber network has been reported as  
64 wound dressing, and showed excellent biocompatibility and degradation rate  
65 commensurate with new tissue formation <sup>22</sup>, suggesting the effect of the network  
66 structure. Currently, commercial regenerated cellulose dressings such as Cellstick<sup>®</sup>  
67 and Cellspan<sup>®</sup> with porous structure are mainly produced by the viscose method <sup>23,24</sup>.  
68 This method still dominates production methods in which pulp with CS<sub>2</sub> is converted  
69 into cellulose xanthogenate with solubility in aqueous sodium hydroxide, which has  
70 been forbidden in many developed countries due to the generation of hazardous  
71 pollutions (CS<sub>2</sub>, H<sub>2</sub>S) during production. In our laboratory, NaOH/urea aqueous  
72 solution precooled to -12°C has been used to dissolve cellulose <sup>25</sup>, and from the  
73 cellulose solution a series of cellulose materials have been successfully fabricated  
74 such as films <sup>26</sup>, hydrogels <sup>27</sup>, fibers <sup>28</sup>, microspheres <sup>29</sup>, and aerogels <sup>30</sup>, through a  
75 green and low-cost process. Thus, a worthwhile endeavor would be to utilize the  
76 cellulose solution to directly prepare a new cellulose dressing with porous structure,  
77 such as sponges which have never been fabricated, and to compare with traditional  
78 cotton gauze. Additionally, gelatin is a natural polymer consisted of complex proteins,  
79 and has been widely used for wound dressing as well as absorbent pad in surgery as a  
80 result of its low antigenicity, high bioabsorptivity, and commercial availability with

---

81 relatively low cost.<sup>31</sup> Meanwhile it is an outstanding carrier for growth factors (e. g.,  
82 bFGF and EGF)<sup>32</sup>, which can promote wound healing. However, gelatin is rarely used  
83 as independent material without cross-linking since its gel-sol transition is at about  
84 37°C in liquid media<sup>33</sup>. On the basis of the hydrogen bonding interaction between  
85 gelatin and cellulose, an efficient strategy to construct composite sponges is by  
86 blending the two natural polymers as wound dressing to avoid the safety problem of  
87 the cross-linking agent usage.

88 In the present work, we provided a green pathway for the producing  
89 cellulose/gelatin composite sponge as wound dressing by changing their aggregation  
90 structure and morphology. The structure and properties of the composite sponges were  
91 characterized by elemental analysis, Fourier transform infra-red (FT-IR) spectra,  
92 solid-state <sup>13</sup>C NMR, scanning electron microscopy (SEM), mechanical testing, water  
93 retention and swelling test. Aiming for wound healing, their growth factor release  
94 ability, cytocompatibility and wound repair ability were also evaluated. A new  
95 pathway to construct effective wound dressing based on cellulose materials is  
96 important for the development and application of highly effective wound dressings to  
97 ease the pain for patients.

98

## 99 **2. Materials and methods**

### 100 **2.1 Materials**

101 Cellulose (cotton linter pulp) with  $\alpha$ -cellulose content of more than 95% was

---

102 provided by Hubei Chemical Fiber Co. Ltd. of China. Its weight-average molecular  
103 weight ( $M_w$ ) was determined by using an Ubbelohde viscometer in a LiOH/urea  
104 aqueous solution at  $25 \pm 0.05^\circ\text{C}$ , and calculated by the equation  $[\eta] = 3.72 \times 10^{-2} M_w^{0.77}$   
105 <sup>34</sup> to be  $1.1 \times 10^5$  g/mol. Gelatin used was derived from porcine skin (type A, powder  
106 approx 300 Bloom, Sigma-Aldrich Co., USA). All other reagents were of analytical  
107 grade and purchased from Sinopharm Chemical Reagent Co., Ltd. of China.

## 108 2.2 Sponge Preparations

109 Cellulose solution was prepared according to the previous method [26]. Cellulose  
110 was dissolved in a mixed solution of NaOH/urea/H<sub>2</sub>O (7:12:81, weight ratio)  
111 precooled to  $-12^\circ\text{C}$  with stirring vigorously for 5 min to obtain a transparent cellulose  
112 solution with 2 wt% concentration. Epichlorohydrin (ECH, 1ml) as a cross-linking  
113 agent was added to the cellulose solution (27g), and the mixture was stirred in an ice  
114 bath for 1 h to yield a homogeneous solution, and then reacted at  $65^\circ\text{C}$  for 2 h. Finally,  
115 the resulted cellulose gels were immersed in deionized water to remove the residual  
116 reagents (NaOH, urea and unreacted ECH) for a week to obtain pure cellulose  
117 hydrogels. The cellulose hydrogels were precooled at  $-20^\circ\text{C}$ , and then freeze-dried by  
118 using a lyophilizer at  $-45^\circ\text{C}$  for 24h to obtain regenerated cellulose sponges material,  
119 coded as RCS.

120 Gelatin was dissolved in aqueous solutions at  $45^\circ\text{C}$  to prepare gelatin solutions  
121 with concentration of 2, 8 and 15 wt%. The cellulose hydrogels mentioned above  
122 were immersed in different gelatin solutions at  $45^\circ\text{C}$  for 24h to obtain  
123 cellulose/gelatin (RCS/G) composite hydrogels. The RCS/G hydrogels were rinsed

---

124 with deionized water to remove the surface gelatin at RT. The hydrogels were  
125 freeze-dried at  $-20^{\circ}\text{C}$  by using a lyophilizer at  $-45^{\circ}\text{C}$  for 24h to obtain the RCS/G  
126 sponges. The RCS/G sponges were coded as RCS/G2, RCS/G8, and RCS/G15,  
127 respectively, according to the gelatin concentrations from 2 to 15 wt%.

128 To fabricate basic fibroblast growth factor (bFGF, Sigma-Aldrich Co., USA) loaded  
129 sponges, a solution of  $1\ \mu\text{gml}^{-1}$  bFGF in PBS was prepared. Dried cylindrical RCS  
130 and RCS/G sponges with diameter of 15 mm and thickness of 2 mm were placed in  
131 24-well plates, and were dropped into 500 $\mu\text{l}$  bFGF solutions. After absorption for 24h  
132 at  $25^{\circ}\text{C}$ , the bFGF loaded sponges were taken out, freeze-dried, and coded as  
133 bFGF-RCS and bFGF-RCS/G, respectively. The bFGF concentration was  
134 quantitatively measured by an enzyme-linked immunosorbent assay (ELISA) kit  
135 (R&D Systems Inc., USA) and enzyme-labeled instrument (Multiskan FC, Thermo  
136 Fisher Scientific Inc., USA) at 450nm. The bFGF left in wells were rinsed by 10 ml  
137 PBS, and their concentrations were analyzed to determine the amounts of bFGF  
138 loaded in sponges.

### 139 **2.3 Characterizations**

140 For Fourier-transform infrared (FT-IR) measurement, the sponges were made into  
141 powder, and then vacuum dried for 24h before characterizations. FT-IR spectra of the  
142 samples pressed into KBr pellets were acquired with a FT-IR spectrometer  
143 (NICOLET 5700, Thermo Fisher Scientific Inc., USA) in the range of  $4000\text{-}500\ \text{cm}^{-1}$ .

144 Solid-state  $^{13}\text{C}$  NMR spectra of the sponge samples were recorded on a Bruker

145 AVANCE-300 NMR system (Bruker Co., Germany) operating at 75 MHz using the  
146 combined technique of proton dipolar decoupling, magic angle spinning (MAS) and  
147 cross-polarization (CP). The spinning rate was set at 5.0 kHz for all samples. The  
148 contact time was 5 ms, the recycle delay 5 s and 5000 scans were accumulated for  
149 each spectrum.

150 The morphologies of the RCS and RCS/G sponges with sputter coated with  
151 platinum were observed by field emission scanning electron microscope (SEM,  
152 Quanta 200, FEI Co., USA) with 15kV accelerating voltage. SEM element mapping  
153 analysis was used to investigate the nitrogen distribution in the RCS/G sponges,  
154 namely gelatin distribution. The pore size ( $d$ ) of the sponges was determined by  
155 measuring samples with 100 pores from the SEM images using the Image J computer  
156 software (National Institute of Health, USA) and averaged.

157 The average nitrogen contents ( $W_N$ , wt %) in the RCS/G sponges were determined  
158 by an elemental analyzer (CHN-O-RAPID, Heraeus Co., Germany). The  $W_N$  values in  
159 different parts of RCS/G sponge were also analyzed to determine the distribution of  
160 gelatin in sponge. The average protein content ( $W_{pro}$ , wt %) of the RCS/G sponges  
161 was calculated by the Kjeldahl method

$$162 \quad W_{pro} = W_N \times 6.25 \quad (1)$$

163 To measure the physical porosities, the RCS and RCS/G sponges were cut into  
164 samples with a size of about 10cm  $\times$  10cm  $\times$  0.7 cm with avoiding excessive  
165 deformation as a result of shear forces. The total volume ( $V$ ) and weight of the dried

166 sponge ( $M$ ) were measured at the same room temperature and humidity, and then the  
167 average density ( $\rho$ ) of the sponge was calculated. The gelatin content ( $W_G$ , wt %) is  
168 equal to  $W_{pro}$ , and the rest of the content is equal to the cellulose content ( $W_{RCS}$ ,  
169 wt %). The density of gelatin ( $\rho_G$ ) and cellulose ( $\rho_C$ ) are 1.35 g/cm<sup>3</sup> and 1.62 g/cm<sup>3</sup><sup>35</sup>,  
170 and then the solid volume of sponge ( $V_S$ ) was calculated by the following equation:

$$171 \quad V_S = M (W_G / \rho_G + W_{RCS} / \rho_C) \quad (2)$$

172 The porosity of the sponge was calculated according to following equation:

$$173 \quad P_r = 1 - V_S / V \quad (3)$$

174 Where,  $P_r$  of each sponge is an average value of three measurements.

#### 175 **2.4 Measurements of physical and mechanical properties**

176 The water retention and swelling degree of the composite sponges as well as gelatin  
177 stability are important for the application. The water retention abilities of sponges  
178 were measured by Ma's method<sup>36</sup>. The sponge samples in the dry state were weighed  
179 and recorded as  $W_{dry}$ . The sample was immersed in phosphate buffered saline (PBS,  
180 pH 7.4) at 37°C for 24h, and then the wet sample was put into a centrifuge tube which  
181 contained filter paper at the button. After centrifugation at 500 rpm for 3 min to  
182 remove the water in the pores, the wet sample was weighted and recorded as  $W_{wet}$ .  
183 The water retention ratio ( $W_{wr}$ ) of sample was calculated by the following formula:

$$184 \quad W_{wr} (\%) = [(W_{wet} - W_{dry}) / W_{dry}] \times 100\% \quad (4)$$

185 The value was an average value of three measurements for each sample.

186 The swelling properties of the sponges were measured by the method as described  
187 as follows. The sample was dried under vacuum at 60°C for 2 h and cooled in a  
188 desiccator. Subsequently, the long side length of sample was measured and coded as  
189  $L_d$ . The sample was then immersed in PBS (pH 7.4) at 37°C for 24h until the sample  
190 reached a constant size. After immersion, the sample was removed from PBS  
191 immediately, and the length of the longer side  $L_w$  was measured. The swelling ratio ( $S$ )  
192 of the sample was calculated by the following equation<sup>37</sup>:

$$193 \quad S (\%) = (L_w - L_d) / L_d \times 100 \quad (5)$$

194 The value was an average value of three measurements for each sample.

195 To further study the gelatin stability in sponge, the RCS/G2 sponges with the same  
196 area were immersed in PBS (pH 7.4) at 37°C for days. At different time intervals, the  
197 samples were taken out and freeze-dried. The nitrogen content changes of samples  
198 were analyzed to calculate the gelatin migration ratio accounting for sponge.

$$199 \quad \text{The gelatin migration ratio} = (W_{N0} - W_{Nt}) \times 6.25 \quad (6)$$

200 Where  $W_{N0}$  and  $W_{Nt}$  were the nitrogen content values of sample before and after  
201 immersed in PBS for  $t$  days, respectively.

202 Unconfined compressive test of the sponges was performed on a universal testing  
203 machine (CMT6503, SANS Test Machine Co. Ltd., China) at room temperature with  
204 a speed of 3 mm min<sup>-1</sup>, according to ASTM 2166-66<sup>38</sup>. Cylindrical-shaped samples  
205 with the size of 20 mm in diameter and 15 mm in height were used. All the samples  
206 were provided with a uniform load, and the compressive strength and modulus values

---

207 were calculated within the linear range of the stress-strain curve. For each sample,  
208 five specimens were tested and the results were averaged.

### 209 **2.5 *In vitro* bFGF release study**

210 The bFGF-loaded sponges were placed in PBS (pH 7.4) and incubated in a shaking  
211 bath (150rpm) at 37°C for different time periods. Periodically, the suspensions were  
212 collected for bFGF analysis, and the releasing media were added by fresh PBS.  
213 Enzyme linked immunosorbent assay ELISA was used to determine the amounts of  
214 bFGF releasing from sponges.

### 215 **2.6 Evaluation of cytocompatibility**

216 The fibroblasts cultures were used to evaluate the cytocompatibility of RCS and  
217 RCS/G sponges. Fibroblasts were derived from rats as reported previously<sup>39</sup>. Briefly,  
218 the skin area of the rats was shaved and disinfected using 75% ethanol. The skin  
219 samples were aseptically removed from the rats and stored in Roswell Park Memorial  
220 Institute (RPMI, Sigma-Aldrich Co., USA) medium, and were then minced into small  
221 pieces to incubate for 3 h in 0.15% collagenase solution (37°C, 5% CO<sub>2</sub>). After  
222 incubation, the samples were centrifuged, the supernatant was discarded and the  
223 precipitation was washed with Dulbecco's modified eagle medium (DMEM, Gibco  
224 Co., USA) supplemented with 10% heat-inactivated fetal bovine serum (FBS, Gibco  
225 Co., USA) for three times. The isolated cells were placed in DMEM medium. After 2  
226 hours, the non-adherent cells were washed out. The cells were incubated in a  
227 humidified incubator in an atmosphere of 5% CO<sub>2</sub> in air.

228 The RCS and RCS/G sponges (25mm in diameter and 2mm in thickness) were  
229 sterilized by ethylene oxide gas at 55°C for 3h. The sterilized sponge samples were  
230 incubated with DMEM medium for 24h before cell seeding, keeping the sponges  
231 infiltrated with DMEM medium. Cells were seeded on each sponge with a cell density  
232 of  $1 \times 10^4$  cells per well and incubated in the incubator (37°C, 5% CO<sub>2</sub>). After the  
233 incubation time for 7 days, 14 days, 21 days, and 28 days, the proliferation of  
234 fibroblasts on (or in) sponges were observed by SEM and fluorescence microscopy  
235 separately.

236 The cytotoxicity of the sponges was measured by the 3-(4,  
237 5-Dimethylthiazol-2-yl)-2, 5-diphenyltetrazoliumbromide (MTT) method. After  
238 incubation for 3 days, MTT (5mg/mL) solutions were added for 4 h, and then the  
239 medium was replaced by Dimethyl Sulphoxide (DMSO, Sigma-Aldrich Co., USA).  
240 The absorbance of DMSO solution was measured at 570 nm using the enzyme-labeled  
241 instrument. The sample containing cells in the culture medium without sponges were  
242 used as control. The relative cell viability in sponge was calculated using the  
243 following equation:

$$244 \quad \text{Cell viability (\%)} = \text{OD}_{570} (\text{sample}) / \text{OD}_{570} (\text{control}) \times 100 \quad (7)$$

245 Where OD<sub>570</sub> value (sample) is obtained in the presence of sponges and OD<sub>570</sub> value  
246 (control) is obtained in the absence of the sponges.

247 For the SEM observations, cell-seeded sponges were prepared as follows: firstly,  
248 the cell-seeded samples were gently rinsed twice with PBS, followed by pre-fixation

---

249 with 2.5% glutaraldehyde (Sigma-Aldrich Co., USA) for 24h. Subsequently, the  
250 samples were rinsed with PBS, followed by post-fixation treatment with 1% osmic  
251 acid (Sigma-Aldrich Co., USA) for 2 h. After washed by PBS three times, the samples  
252 were dehydrated in ethanol gradient (30%, 50%, 70%, 80%, 90%, 95% and 100%)  
253 respectively. After drying in a critical point dryer, the cell-seeded samples were  
254 sputter coated with gold, observed by field emission scanning electron microscope  
255 (SIRION TMP, FEI Co., USA) and photographed. To prepare cell-seeded sample for  
256 fluorescence microscopy observation, the cultured sponges were rinsed three times  
257 with PBS, and the cells in sponges were labeled by calcein-AM and pro-pidium iodide  
258 (PI) (Sigma-Aldrich Co., USA). Fluorescent images of the stained samples were  
259 obtained using a florescent microscope (Axio Observer Z1, Zeiss Co., Germany).

## 260 **2.7 Animal Test**

261 The weights of twelve New Zealand rabbits (6 females and 6 males) were between  
262 2.25 and 2.50 kg at the time of experiment, and were purchased from the Laboratory  
263 Animal Center of Wuhan University and used in the animal test. The animals were  
264 divided into two groups, each with 3 females and 3 males. Rabbits were anesthetized  
265 by Nembutal injection (0.3ml/kg) for surgery and creation of wounds. Each group was  
266 responsible for the partial-thickness and full-thickness cutaneous wound, respectively.  
267 According to the depth of the wound, partial-thickness and full-thickness skin wounds  
268 for group 1 and group 2 were separately prepared by removing skin area with surgical  
269 scissors and forceps. For eliminating the interference of individual difference, four  
270 skin wounds (20mm × 20mm) were made on dorsum of each rabbit and arranged

---

271 symmetrically. The wounds for rabbits were treated with RCS, RCS/G2 and  
272 bFGF-RCS/G2 sponges with gauze as control, and then fixed with a polyurethane  
273 film coated a binder material polyacrylic acid (Fulong Co., China) by surgical suture.  
274 During the experiment, all rabbits showed good health condition. The wounds were  
275 photographed to measure the areas of wounds at different time intervals. All animal  
276 experiments in our study were carried out in accordance with the guideline and ethics  
277 approval of the Laboratory Animal Center of Wuhan University.

### 278 **2.8 Histological Analysis**

279 At certain intervals, wound tissue samples were fixed in formalin and embedded in  
280 paraffin (Sinopharm Chemical Reagent Co., Ltd., China) for routine histological  
281 processing. The 3-5  $\mu\text{m}$  sections of each paraffin block were stained with hematoxylin  
282 and eosin (H&E) and observed by a light microscope.

### 283 **2.9 Statistical Analysis**

284 Statistical analysis was performed by the PASW Statistics 18 software package  
285 (IBM Co., USA). The data were analyzed statistically with Duncan's multiple  
286 range tests. The differences between groups were considered to be statistically  
287 significant,  $P$  values  $<0.05$  level, which indicates that the means are significantly  
288 different when compared with the control group.

289

290

291

292

### 293 **3 Results and Discussion**

#### 294 **3.1 The structure and morphology of sponges**

295 The IR spectra of the RCS and RCS/G sponges are shown in Figure 1a. The OH  
296 stretching vibration bands around  $3420\text{ cm}^{-1}$  in the RCS sponge were broadened and  
297 shifted to a lower wavenumber in the RCS/G sponges, suggesting the formation of  
298 new hydrogen bonds between the gelatin and cellulose macromolecules. Compared  
299 with RCS, the carbonyl group (amide I bond) at  $1654\text{ cm}^{-1}$  of gelatin in the RCS/G  
300 sponges shifted to a lower wavenumber. Moreover, the relative intensity at  $1544\text{ cm}^{-1}$   
301 (amide II bond) of gelatin also appeared in RCS/G sponges, and the band broadened  
302 and shifted to lower wavenumbers, comparing with gelatin. These changes of relative  
303 intensity without new peak formation in RCS/G spectra indicated the existence of the  
304 intermolecular hydrogen bonds between gelatin and cellulose.

305 Figure 1b shows the solid-state  $^{13}\text{C}$  NMR spectra of RCS and RCS/G sponges. There  
306 were four significant peaks at 105.8, 88.0, 73.2 (75.0, 72.5), 63.3 ppm in the spectrum  
307 of the RCS sponge, assigned to the C1, C4, C5 (C3, C2), C6 of the cellulose  
308 molecules. The peak assignment of gelatin was carried out in accordance with earlier  
309 reports<sup>40</sup>. No new peaks appeared in the spectra of the RCS/G sponge, suggesting that  
310 no derivatization occurred. The  $^{13}\text{C}$  NMR spectra of RCS/G sponge revealed the same  
311 cellulose signal peaks, whereas that assigned to the glycine (Gly  $\alpha$ ) and  
312 hydroxyproline (Hyp  $\gamma$ ) disappeared. Glycine and hydroxyproline were polar amino

---

313 acids in gelatin, resulting in extraordinarily strong hydrogen bonds with cellulose. The  
314 amino group of glycine could easily form hydrogen bonds with the hydroxyl group of  
315 cellulose, leading to the decrease of signal expression in RCS/G sponge. On the basis  
316 of the above results, it can be inferred that strong interactions between cellulose and  
317 gelatin occurred through hydrogen bonding between the hydroxyl groups of cellulose  
318 and the amino groups of gelatin in RCS/G.

319 The results of average nitrogen contents ( $W_N$ ) and protein content ( $W_{pro}$ ) of the RCS  
320 sponges are summarized in Table 1. The  $W_N$  value of RCS was 0, indicating that the  
321 urea was completely removed from the hydrogel by washing treatment, so the  $W_N$   
322 values in RCS/G sponges could only be due to the existence of gelatin. With an  
323 increase of the concentration of the gelatin solution, the  $W_N$  and protein content of the  
324 RCS/G sponges increased. Therefore, the porous structure of cellulose hydrogels  
325 could provide not only the cavities for the penetration of the gelatin molecules, but  
326 also the compatible support to combine gelatin. Namely, cellulose hydrogel could  
327 absorb abundant gelatin molecules, and the gelatin content of the RCS/G sponges can  
328 be adjusted by changing the gelatin concentrations.

329 Figure 2 shows the photographs and surface SEM images of the RCS and RCS/G  
330 sponges, and Figure S1 displayed the cross-section SEM images of sponge. All of the  
331 sponges were of white color exhibited porous structure. The average pore size ( $d$ ) of  
332 the RCS sponge was about 97 $\mu\text{m}$ , and the pore size slightly increased with an increase  
333 of the gelatin content (as shown in Table 1). This could be explained by the  
334 hydrophilicity of gelatin which induced more H<sub>2</sub>O molecules to be stored in the

335 RCS/G hydrogel, leading to the formation of bigger ice crystals in the RCS/G  
336 hydrogel at  $-20^{\circ}\text{C}$ , resulting in the larger pores. On the other hand, when gelatin  
337 content achieved 46%, the average pore size of RCS/G15 sponge was reduced to 85  
338  $\mu\text{m}$ . It was not hard to imagine that large amount of gelatin attached on the pore walls  
339 of cellulose, further leading to the increasing thickness of the pore walls and the  
340 decreasing of pore space. Moreover, the porosity ( $P_r$ ) values of the RCS and RCS/G2  
341 sponges were above 90%, whereas excess gelatin filled into pores led to the sharp  
342 decrease of  $P_r$ . According to the above results, the RCS/G sponge possessed macro-  
343 and micro porous architecture, which could keep the gas exchange on the wound  
344 interface.

345 To further determine the distribution of gelatin in RCS/G sponge, the cross-section  
346 of the RCS/G2 sponges were divided as the external (①), internal (②) and internal  
347 center (③) regions, as shown in Figure 3a. The  $W_N$  contents of samples had difference,  
348 demonstrating that the gelatin distribution in the RCS/G2 sponge decreased from  
349 external to center (Figure 3b). Setting RCS sponge as a control, the N signal in  
350 element mapping images of the RCS/G sponge was from gelatin (Figure 3c). These  
351 element mapping images were consistent with the results of element analysis. This  
352 difference gelatin distribution in sponge owed to the gelatin diffusion gradient.  
353 Combined with SEM images and element mapping images, large amount of gelatin  
354 was found to attach on the pore walls of cellulose.

### 355 **3.2 Water retention ability, gelatin stability and mechanical properties of sponges**

356 The water retention ability of wound dressing is relative to absorb body fluids, to

---

357 transform cell nutrients and metabolites, and to keep a moist environment for  
358 promoting wound repair. After absorption in the PBS solution for 2 min, the RCS/G  
359 sponge keep abundant solution and exhibited flexibility, which was beneficial for  
360 absorbing the exudates and fitting the wound surface (Figure 4a). It was noted that  
361 after immersion in PBS, gauze displayed solution leakage due to its loose weave  
362 structure (Figure S2). The water retention ratio values ( $W_{wr}$ ) of the RCS and  
363 composite sponges were in the range of 700-800% (Table 1), suggesting that the  
364 sponges could hold water as much as several times of their own weight. Therefore, the  
365 macro- and micro pores of the sponges could not only hold abundant liquids, and also  
366 keep moist environment for effective wound repair. Furthermore, the presence of  
367 gelatin with amino and carboxyl groups also increased the water retention ability  
368 (Table 1). Usually, excessive change in size can induce separation of the dressing  
369 from the skin outside of the wound area, and the leakage of fluid, leading to  
370 enlargement of the wound due to the invasion of microorganisms.<sup>41</sup> In our findings,  
371 the  $S$  values of RCS/G2 and RCS/G8 sponges were below 10%, which could be  
372 accepted as wound dressings. Therefore, the RCS/G sponges could have both  
373 excellent water retention capacity and dimensional stability, indicating the good  
374 candidates for wound dressings. As in Figure S3 shown, the migration ratio of gelatin  
375 migrated from sponge after immersed in PBS (pH 7.4) at 37°C for 14 days accounts  
376 for 4.6% of the sponge. According to the result of the average nitrogen content of  
377 RCS/G2 (29.2%), less than 16% gelatin was dissolved in PBS. The large amount  
378 gelatin still kept stability in the composite sponge due to the hydrogen bonding

---

379 interactions between gelatin and cellulose, which could contribute to the combination  
380 with growth factors.

381 As a candidate for wound dressings, the mechanical properties of sponges are  
382 important. The results of mechanical testing are listed in Table 2. The compressive  
383 strength values of RCS and RCS/G sponges were much higher than that of chitosan <sup>42</sup>,  
384 alginate <sup>43, 44</sup>, collagen <sup>42</sup> and silk <sup>45</sup>. The compressive moduli and strength of the  
385 composite sponges increased with the increase of the gelatin content, indicating  
386 further the strong interactions between gelatin and cellulose. Therefore, the RCS and  
387 RCS/G sponges exhibited excellent mechanical properties, which were beneficial to  
388 be used as dressing or scaffold for wound healing.

### 389 **3.3 The bFGF sustained release and cytocompatibility of sponges**

390 Basic fibroblast growth factor (bFGF) can stimulate the proliferation of fibroblasts  
391 and endothelial cells to promote angiogenesis and wound healing. However, the direct  
392 use of bFGF usually results in relatively low activity due to the short half-life of  
393 bFGF <sup>46</sup>. By ELISA assay and calculations, as given the same amount of bFGF  
394 (500ng) for RCS and RCS/G2 sponges with the same size (cylindrical shape of  
395 sponges with diameter of 15 mm and thickness of 2 mm), the bFGF can connect with  
396 them, and the loading on the RCS/G2 sponge (330±10 ng) was higher than that on  
397 RCS sponge (274±12 ng). This could be explained that the gelatin containing amino  
398 acids has more bonding points with bFGF through the electrostatic and  
399 hydrogen-bond interactions <sup>47,48</sup>. To figure out the bFGF release from the sponges and  
400 evaluate the possibility as a functional wound dressing with releasing growth factors,

---

401 their release abilities were evaluated by the *in vitro* test. Compared with RCS, bFGF  
402 in RCS/G2 exhibited a sustained and steady release and the cumulative release mass  
403 was approximately 84% until 21 days (as shown in Figure 4b). Therefore, sustained  
404 release of bFGF in RCS/G sponge contributed to the strong interactions between  
405 gelatin and bFGF. For clinical applications, the RCS/G2 sponge was found to be more  
406 desirable since the release of the growth factor matched the wound healing period and  
407 provided a sustained release to the target area.

408 To evaluate the applicability of sponges for wound healing, the cytocompatibility of  
409 sponges was studied by *in vitro* cell culture test. The morphologies of fibroblasts  
410 cultured on sponges for 3 days are shown in Figure 5a-d. The fibroblasts attached and  
411 spread well both on the RCS and RCS/G sponges, indicating that the environment of  
412 the sponges was beneficial for cells growth. To further clarify their cytocompatibility,  
413 the MTT test was also performed (Figure S4). The cell viability values of the RCS,  
414 RCS/G2 and RCS/G8 sponges were all above 80%, confirming that these sponges did  
415 not have acute cytotoxic effect. Moreover, the cell viability values of RCS/G2 and  
416 RCS/G8 were higher than RCS, showing the effect of gelatin to promote cell growth.  
417 However, RCS/G15 sponge with 46% gelatin content exhibited only 70% cell  
418 viability. This could be explained that the excess gelatin can block the pathways for  
419 transformation of cell nutrients and metabolites. As shown in Figure 5e-h, the cells  
420 displayed more profuse proliferation on RCS and RCS/G2 sponges and almost  
421 occupied the pore walls of sponges after culture for 14 days, as a result of the role of  
422 the porous structure. To further assess the cell growth in sponges, fluorescence

---

423 microscopy was used to observe the calcein-AM and PI labeled fibroblasts in sponges  
424 (Figure S5). The sponges displayed a number of live cells, in consistent with the result  
425 of MTT test and SEM observation. Therefore, the gelatin incorporation with an  
426 appropriate amount (< 46 wt%) into cellulose could further promote cell growth,  
427 leading to good biocompatibility.

### 428 **3.4 Evaluation of *in vivo* wound healing**

429 The healing of wounds treated with RCS, RCS/G2 and bFGF-RCS/G2 sponges  
430 were evaluated by *in vivo* wound healing experiments on rabbits, using gauze as a  
431 control (Figure S6). Figure 6a-b shows the wound healing observation and the  
432 changes of the partial-thickness wound area treated with sponges. The healing rate of  
433 gauze-treated wound was the slowest, compared with all other sponges. After 12 days,  
434 the area of wound treated with bFGF-RCS/G2 sponges was 0.6 cm<sup>2</sup>, exhibiting 85%  
435 wound closure. In comparison with RCS sponge, the bFGF and RCS/G2 sponges  
436 exhibited, respectively, the best and better healing effect. This could be due to the  
437 excellent ability of bFGF in promoting wound healing, and gelatin still retained some  
438 signals such as Ary-Gly-Asp (RGD) sequence of collagen, promoting cell adhesion,  
439 proliferation and differentiation<sup>49</sup>. Figure 6c-d shows the wound healing observation  
440 and the changes of the full-thickness wound area treated with sponges. Clearly, the  
441 healing rate of the gauze-treated wounds was also lower than all sponges. The wound  
442 treated with the bFGF-RCS/G2 sponge also displayed the fastest healing rate.  
443 Interestingly, the complete wound healing time for the wounds treated with  
444 bFGF-loaded sponges was 7 days faster than that treated with traditional cotton gauze

---

445 for full-thickness coetaneous wound model, which could substantially ease the pain  
446 for the patients. On the whole, cellulose based-sponges (RCS, RCS/G2 and  
447 bFGF-RCS/G2) exhibited much more effective wound repair abilities than gauze.  
448 Especially, since the RCS sponges were derived from cellulose, same as gauze. Why  
449 is there such clear difference in wound repairing between them? It was not hard to  
450 imagine that the macro- and micro-porous structure with thin pore wall in the sponges  
451 played an important role in the improvement in absorbing the wound exudates, the gas  
452 exchange and to maintain a moist environment for wound repair. However, gauze  
453 weaved from cellulose fibers with small specific area, which not only ineffectively  
454 absorbs excess exudates, but also fails in water retention (Figure S2).

455 As shown in Figure 7a-b, the RCS/G2 sponge was removed easily from the wound,  
456 keeping intact the wound surface. However, cotton gauze adhered to the wound  
457 surface when removed, leading to secondary injuries (Figure 7c-d). The excellent  
458 water retention ability of the sponge and the minimal contact interface between the  
459 sponge and the wound (due to thin pore wall of about 1-5 $\mu$ m estimated by SEM) were  
460 the possible reasons that facilitated the easy-peeling ability of sponges as showed in  
461 (Figure 7e). Very different from sponge, the minimal contact interface between gauze  
462 and skin wound was a cotton fiber with the diameter of about 300-400  $\mu$ m.

### 463 **3.5 Histological Analysis**

464 Generally, wound healing is a complex process involving a series of interrelated  
465 and overlapped steps, such as hemostasis, inflammation, cell migration and  
466 proliferation, angiogenesis, neovascularization, extracellular matrix (collagen)

---

467 production and remodeling <sup>12</sup>. In this work, the wound tissues were biopsied and  
468 processed for histological examination to evaluate the progress of wound healing.  
469 Figure 8 shows the histopathological changes of the wound tissues as a function of  
470 time. For partial-thickness wounds on day 3, the wounds treated with bFGF-RCS/G2  
471 sponges exhibited less inflammation cells and neovascularization scores than the  
472 wound treated with cotton gauze and RCS sponge. Furthermore, compared with  
473 cotton gauze, more new capillaries around the inflammatory cells were observed in  
474 the wounds treated with RCS sponges, indicating more effective wound repair by  
475 sponges. After 7 days, a continuous nascent epithelial layer was formed, namely  
476 epidermis, on the wounds treated with the RCS, RCS/G2 and bFGF-RCS/G2 sponges  
477 with an appearance more mature than those treated with gauze. Especially, after  
478 treated with the bFGF-RCS/G2 sponge, the bundles of collagen fibers were observed  
479 to be loose and wavy in the dermis tissue, suggesting that the excellent promotion  
480 provided by bFGF. For full-thickness wounds, a large number of inflammatory cells  
481 were observed in the wounds after 3 days. However, a continuous nascent epithelial  
482 layer and some collagen fibers started to form over the wounds with the treatments of  
483 RCS/G2 and bFGF-RCS/G2 sponges after 19 days, indicating complete healing. In  
484 particular, the great formation of blood vessels and well-proliferated fibroblasts  
485 occurred on the wound for bFGF-RCS/G2 sponges. The inflammatory cell number on  
486 the wounds treated with RCS sponge was clearly decreased on day 19. However, the  
487 wound treated with cotton gauze had many inflammatory cells, indicating the healing  
488 process was still in the inflammatory phase. On the basis of the results mentioned

---

489 above, both the full thickness and partial-thickness wounds indicated that the RCS/G2  
490 and bFGF-RCS/G2 sponges as potential dressings could provide suitable environment  
491 for a rapid and complete wound healing. It was demonstrated that the macro- and  
492 micro-pores with thin wall in the sponges provided the cavities and channels for gas  
493 exchange, exudates absorption and water retention, this is very important for the  
494 wound healing. In addition, gelatin in the sponge not only promoted fibroblasts  
495 proliferation and differentiation, but also facilitated the sustained release of bFGF,  
496 resulting in the formation of neovascularization and collagen fiber.

497 In view of the results mentioned above, a scheme describing the mechanism that  
498 bFGF-RCS/G sponge promotes wound healing is proposed in Figure 9. The  
499 bFGF-RCS/G sponge was consisted of cellulose as porous support and gelatin as filler,  
500 supported by SEM observation in Figures 2b1-c4 and S1. The macro- and micro-  
501 pores of the sponges induced the gas exchange, absorb excess wound exudates and  
502 maintain moist environment around the wound area, supported by the results in  
503 Figures 6-8. Gelatin combined to the pore walls of cellulose not only promoted cell  
504 growth, but also achieved a sustained release of bFGF to stimulate collagen synthesis  
505 <sup>50</sup>, promoted cell proliferation and neovascularization <sup>51</sup>, leading to a rapid and  
506 effective wound repair (as supported by the results in Figures 3-8). The bFGF and  
507 gelatin were immobilized in the cellulose sponge through hydrogen bonding, retaining  
508 their inherent biocompatibility, so they can significantly promote wound healing.

509

510

511

**512 4. Conclusion**

513 The cellulose/gelatin composite sponges for wound healing were successfully  
514 fabricated by immersing the cellulose hydrogels in the gelatin solutions and followed  
515 by freeze-drying process via a simple, green and cost-effective pathway. Compared  
516 with cotton gauze, the cellulose sponge having the same chemical structure effectively  
517 promoted wound healing, as a result of the macro- and micro porous architecture.  
518 Furthermore, the gelatin and basic fibroblast growth factor were immobilized in the  
519 cellulose sponge through hydrogen bonding to retain their inherent biocompatibility,  
520 leading to the excellent repairing efficacy. The incorporation of gelatin not only  
521 promoted cell growth, but also achieved the sustained release of growth factors from  
522 sponge, resulting in rapid wound healing. For the full-thickness coetaneous wound  
523 model, the complete wound healing time for the wounds treated with bFGF-loaded  
524 cellulose sponges was 7 days faster than that treated with gauze. The pores with thin  
525 wall in the sponges played an important role to hasten up the healing process, as a  
526 result of satisfying the requirements of oxygen permeability, controlled water vapor  
527 evaporation and wound exudates absorption. The cellulose composite sponges  
528 exhibited the highly effective wound healing, this is important for the successful  
529 application of the wound dressings based on cellulose materials.

530

**531 Acknowledgments**

532 This work was supported by the National Basic Research Program of China (973

533 Program, 2010CB732203), the Major Program of National Natural Science  
534 Foundation of China (21334005) and the National Natural Science Foundation of  
535 China (20874079).

## 536 Reference

- 537 1 T. G. Weiser, S. E. Regenbogen, K. D. Thompson, A. B. Haynes, S. R. Lipsitz, W. R. Berry and A.  
538 A. Gawande, *Lancet.*, **2008**, 372,139.
- 539 2 R. Jayakumar, M. Prabakaran, P. T. S. Kumar , S. V. Nair and H. Tamura, *Biotechnol. Adv.*, **2011**,  
540 29, 322.
- 541 3 G. D. Mogosanu and A. M. Grumezescu, *Int. J. Pharm.*, **2014**, 463,127.
- 542 4 Y. F. Goh, I. Shakir and R. Hussain, *J. Mater. Sci.*, **2013**, 48, 3027.
- 543 5 Z. Fan, B. Liu, J. Wang, S. Zhang, Q. Lin, P. Gong, L. Ma and S. Yang, *Adv. Funct. Mater.*, **2014**,  
544 24, 3933.
- 545 6 V. Ambrogi, A. Donnadio, D. Pietrella, L. Latterini, F. A. Proietti, F. Marmottini, G. Padeletti, S.  
546 Kaciulis, S. Giovagnoli and M. Ricci, *J. Mater. Chem. B*, **2014**, 2, 6054.
- 547 7 H. Lai, C. Kuan, H. Wu, J. C.Tsai, T. Chen, D. J.Hsieh and T. Wang, *Acta Biomater.*, **2014**, 10,  
548 4156.
- 549 8 R. A.Thakur, C. A. Florek, J. Kohn and B. B. Michniak, *Int. J. Pharm.*, **2008**, 364, 87.
- 550 9 S. Rastogi, M. Modi and B. Sathian, *J. Oral Maxillofac Surg.*, **2009**, 67,1600.
- 551 10 L.Yunki, J. W. Bae, J. W. Lee, W. Suh and K. D. Park, *J. Mater. Chem. B.*, **2014**, 2, 7712.
- 552 11 M. Kempf, Y. Miyamura, P. Liu, A. C. H. Chen, H. Nakamura, H. Shimizu, Y. Tabata, R. M.  
553 Kimble and J. R. McMillan, *Biomaterials*, **2011**, 32, 4782.
- 554 12 A. Schneider, X. Wang, D. L. Kaplan, J. A. Garlick and C. Egles, *Acta Biomater.*, 2009, 5, 2570.
- 555 13 L. Fu, J. Zhang and G. Yang, *Carbohydr. Polym.*, **2013**, 92, 1432.
- 556 14 K. Murakami, H. Aoki, S. Nakamura, S. Nakamura, M. Takikawa, M. Hanzawa, S. Kishimoto, H.  
557 Hattori, Y. Tanaka, T. Kiyosawa, Y. Sato and M. Ishihara, *Biomaterials*, **2010**, 31, 83.
- 558 15 A. Svensson, E. Nicklasson, T. Harrah, B. Panilaitis, D. L. Kaplan, M. Brittberg and P. Gatenholm,  
559 *Biomaterials*, **2005**, 26, 419.
- 560 16 C. Brackmann, A. Bodin, M. Akeson, P. Gatenholm and A. Enejder, *Biomacromolecules*, **2010**, 11,  
561 542.
- 562 17 S. Ponader, H. Brandt, E. Vairaktaris, C. von Wilmowsky, E. Nkenke, K. A. Schlegel, F. W.  
563 Neukam, S. Holst, F. A. Muller and P. Greil, *Colloids Surf. B Biointerfaces*, **2008**, 64, 275.
- 564 18 M. I. Montanez, E. Perez-Inestrosa, R. Suau, C. Mayorga, M. J. Torres and M. Blanca ,  
565 *Biomacromolecules*, **2008**, 9, 1461.

- 
- 566 19 S. A. Hutchens, R. S. Benson, B. R. Evans, H. M. O'Neill and C. J. Rawn, *Biomaterials*, **2006**, 27,  
567 4661.
- 568 20 Q. Shi, L. Yang, J. Sun, H. Zhang, L. Chen, B. Chen, H. Yang and Z. Wang, *Biomaterials*, **2012**, 33,  
569 6644.
- 570 21 J. V. M. Märtson, T. Hurme, P. Laippala and P. Saukko, *Biomaterials*, **1999**, 20, 1989.
- 571 22 W. Czaja, A. Krystynowicz, S. Bielecki and R. M. Brown, *Biomaterials*, **2006**, 27, 145.
- 572 23 T. Miyamoto, S. Takahashi, H. Ito, H. Inagaki and Y. Noishiki, *J. Biomed. Mater. Res.*, **1989**, 23,  
573 125.
- 574 24 D. Klemm, B. Heublein, H. P. Fink and A. Bohn, *Angew. Chem. Int. Edit.*, **2005**, 44, 3358.
- 575 25 J. Cai, L. Zhang, S. Liu, Y. Liu, X. Xu, X. Chen, B. Chu, X. Guo, J. Xu, H. Cheng, C. Han and S.  
576 Kuga, *Macromolecules*, **2008**, 41, 9345.
- 577 26 H. Qi, C. Chang and L. Zhang, *Green Chem.*, **2009**, 11, 177.
- 578 27 Z. Wang, X. Fan, M. He, Z. Chen, Y. Wang, Q. Ye, H. Zhang and L. Zhang, *J. Mater. Chem. B*,  
579 **2014**, 2, 7559.
- 580 28 J. Cai, L. Zhang, J. Zhou, H. Qi, H. Chen, T. Kondo, X. Chen and B. Chu, *Adv. Mater.*, **2007**, 19,  
581 821.
- 582 29 J. Duan, X. He and L. Zhang, *Chem. Commun.*, **2015**, 51, 338.
- 583 30 Z. Shi, H. Gao, J. Feng, B. Ding, X. Cao, S. Kimura, Y. Wang, L. Zhang and J. Cai, *Angew. Chem.*  
584 *Int. Edit.*, **2014**, 53, 5380.
- 585 31 S. M. Lien, L. Y. Ko and T. J. Huang, *Acta Biomater.*, **2009**, 5, 670.
- 586 32 S. Young, M. Wong, Y. Tabata and A. G. Mikos, *J. Control. Release.*, **2005**, 109, 256.
- 587 33 Y. Zhang, H. W. Ouyang, C. T. Lim, S. Ramakrishna and Z. Huang, *J. Biomed. Mater. Res. B*,  
588 **2005**, 72B, 156.
- 589 34 J. Cai, Y. Liu and L. Zhang, *J. Polym. Sci. B: Polym. Phys.*, **2006**, 44, 3093.
- 590 35 X. Liu and P. Ma, *Biomaterials*, **2009**, 30, 4094.
- 591 36 J. Ma, H. Wang, B. He and J. Chen, *Biomaterials*, **2001**, 22, 331.
- 592 37 K. Katoh, T. Tanabe and K. Yamauchi, *Biomaterials*, **2004**, 25, 4255.
- 593 38 *ASTM standard 2007*, Standard test method for unconfined compressive Test.
- 594 39 A. Blasinska and J. Drobnik, *Biomacromolecules*, **2008**, 9, 776.
- 595 40 D. Huster, J. Schiller and K. Arnold, *Magn. Reson. Med.*, **2002**, 48, 624.
- 596 41 A. Ralph, W. W. H. Meyer and A. S. James, *US Patent*, No 4738257 A, **1988**.
- 597 42 S. C. Y. Kim, E. Kang, I. Kwon, E. Lee, J. Kim, H. Chung and S. I. Jeong, *Fiber Polym.*, **2001**, 2,  
598 64.
- 599 43 J. Han, Z. Zhou, R. Yin, D. Yang and J. Nie, *Int. J. Biol. Macromol.*, **2010**, 46, 199.
- 600 44 C. Wang, K. Yang, K. Lin, H. Liu and F. Lin, *Biomaterials*, **2011**, 32, 7118.

- 
- 601 45 R. Nazarov, H. J. Jin and D. L. Kaplan, *Biomacromolecules*, **2004**, 5, 718.
- 602 46 R. Langer, *Science*, **1990**, 249, 1527.
- 603 47 Y. Tabata, A. Nagano, M. D. Muniruzzaman and Y. Ikada, *Biomaterials*, **1998**, 19, 1781.
- 604 48 Y. Tabata and Y. Ikada, *Adv. Drug Deliv. Rev.*, **1998**, 31, 287.
- 605 49 C. Chang, H. Liu, C. Lin, C. Chou and F. Lin, *Biomaterials*, **2003**, 24, 4853.
- 606 50 M. Imamura, A. Kanematsu, S. Yamamoto, Y. Kimura, I. Kanatani, N. Ito, Y. Tabata and O.  
607 Ogawa, *Am. J. Physiol. Renal. Physiol.*, **2007**, 293, F1007.
- 608 51 S. Barrientos, O. Stojadinovic, M. S. Golinko, H. Brem and M. Tomic-Canic, *Wound Repair*  
609 *Regen.*, **2008**, 16, 585.
- 610

---

## 611 **Figure captions**

612 **Figure 1.** FT-IR (a) and solid state  $^{13}\text{C}$  NMR (b) spectra of RCS, gelatin and RCS/G sponges.

613 **Figure 2.** The photographs of RCS and RCS/G sponges at the dry state (a), and the surface SEM  
614 images of RCS(b1, c1), RCS/G2 (b2, c2), RCS/G8 (b3, c3) and RCS/G15 (b4, c4), the bar for  
615 b1-b4:20  $\mu\text{m}$  and the bar for c1-c4:10 $\mu\text{m}$ .

616 **Figure 3.** Scheme to describe the external (①), internal (②) and internal center (③) regions of the  
617 cross-section of the RCS/G2 sponge (a), the nitrogen content ( $W_N$ , wt %) (b), the SEM images and  
618 the nitrogen element mapping images (c) of the RCS and RCS/G2 sponges, corresponding to the  
619 ①, ② and ③ regions in (a).

620 **Figure 4.** The photograph of RCS/G2 sponge after being immersed in PBS solution for 2 min (a),  
621 the bar is 1 cm. Cumulative bFGF release from RCS and RCS/G2 sponges (b), and individual  
622 points represent the mean values  $\pm$  standard deviation (SD) from three sponges samples.

623 **Figure 5.** RCS (a, e), RCS/G2(b, f), RCS/G8(c, g) and RCS/G15(d, h) sponges seeded with  
624 fibroblasts for 3 days (a-d) and 14 days (e-h) of culture. The bar is 50 $\mu\text{m}$ .

625 **Figure 6.** The wound closure of partial-thickness (a) and full-thickness (c) wounds treated with  
626 gauze, RCS sponge, RCS/G2 sponge and bFGF-RCS/G2 sponge for days. The initial area of all  
627 wounds on each rabbit was 4  $\text{cm}^2$ , and the bar is 2 cm. Evaluation of the partial-thickness (b) and  
628 full-thickness wound area (d). The data represent the mean  $\pm$  SD of six rabbits. (\*  $P < 0.05$ ,  
629 compared to control for same day).

630 **Figure 7.** RCS/G2 sponge has easy-peeling property (a), preventing the secondary injury when  
631 removed from the wound (b); cotton gauze adheres to the wound surface when peeled (c), leading  
632 to the secondary injury (d); the schematic of interface between the sponge and the skin wound  
633 (e).

634 **Figure 8.** Histological images of skin tissues stained by hematoxylin and eosin (H&E) method  
635 dissected in the post-operative day 3 (a1-d1) and day 7 (a2-d2) for partial-thickness wound, and in  
636 day 3 (a3-d3) and day 10 (a4-d4) for full-thickness wound, respectively. The groups were RCS (b),  
637 RCS/G2 (c), bFGF-RCS/G2 (d) sponges treated wound, and the medical cotton gauze (a) treated

---

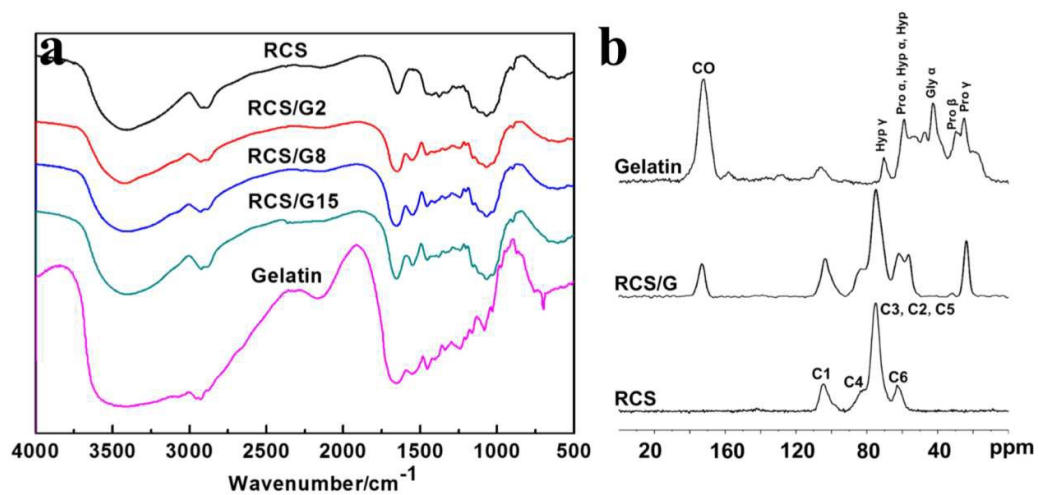
638 wound was used as control. Scar bar is 100 $\mu$ m. The arrow, triangle and star represent blood vessel,  
639 epidermis, collagen fibers, respectively.

640 **Figure 9.** The mechanism scheme to describe the promoting wound repair of bFGF-RCS/G  
641 sponges.

642 **Table 1.** The average nitrogen content ( $W_N$ , %), the average protein content ( $W_{Pro}$ , %), porosity  
643 ( $P_r$ , %), water retention ratio ( $W_{wr}$ , %), the average pore size ( $d$ ,  $\mu$ m) and swelling ratio ( $S$ , %) of  
644 the RCS and RCS/G sponges.

645 **Table 2.** The compressive moduli (kPa) and compressive strength (kPa) of RCS sponge, RCS/G  
646 sponges, and porous scaffolds or sponges derived from other natural polymers.

647

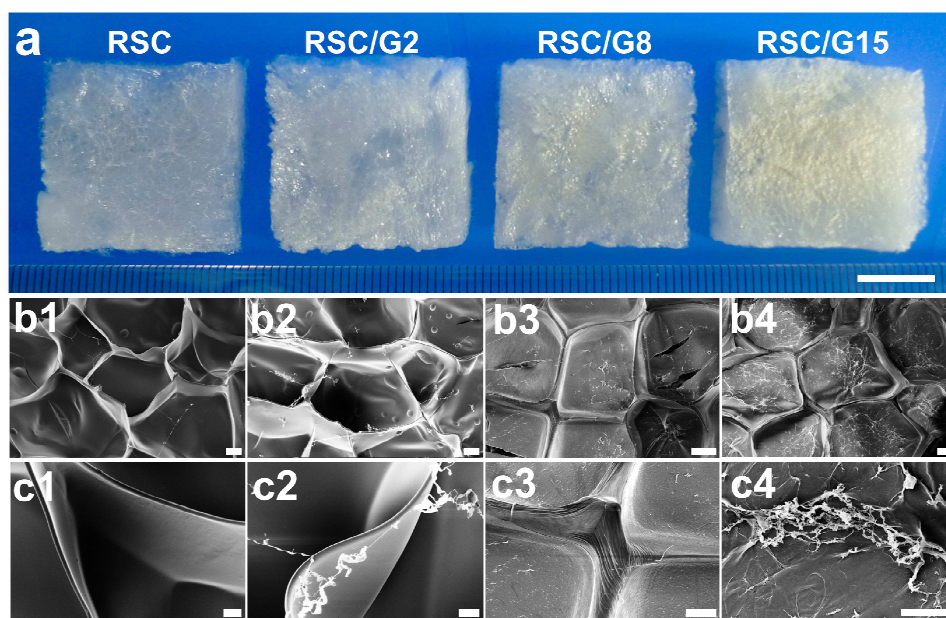


648

649 **Figure 1.** FT-IR (a) and solid state <sup>13</sup>C NMR (b) spectra of RCS, gelatin and RCS/G sponges.

650

651

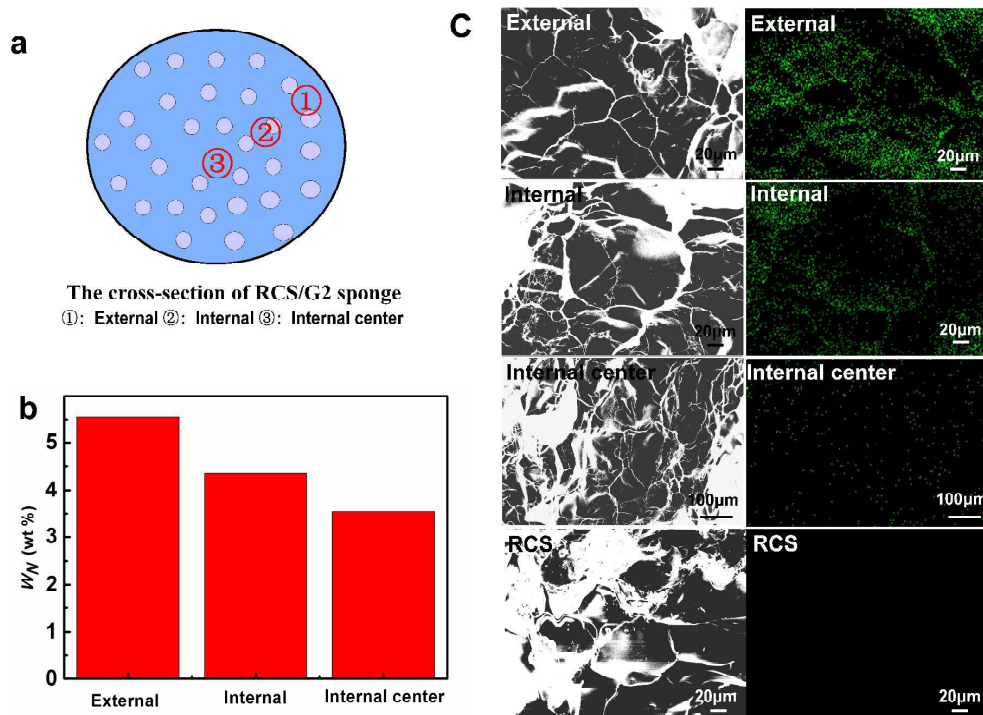


652

653 **Figure 2.** The photographs of RCS and RCS/G sponges at the dry state (a), and the surface SEM  
654 images of RCS(b1, c1), RCS/G2 (b2, c2), RCS/G8 (b3, c3) and RCS/G15 (b4, c4), the bar for  
655 b1-b4:20  $\mu\text{m}$  and the bar for c1-c4:10 $\mu\text{m}$ .

656

657

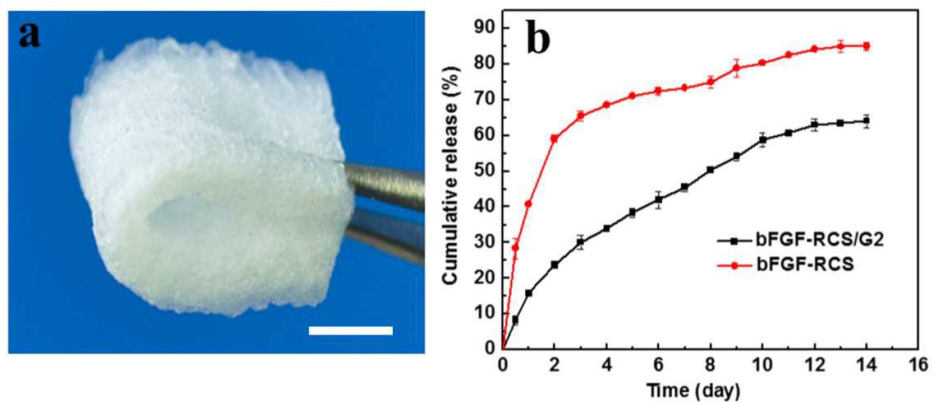


658

659 **Figure 3.** Scheme to describe the external (①), internal (②) and internal center (③) regions of the  
 660 cross-section of the RCS/G2 sponge (a), the nitrogen content ( $W_N$ , wt %) (b), the SEM images and  
 661 the nitrogen element mapping images (c) of the RCS and RCS/G2 sponges, corresponding to the  
 662 ①, ② and ③ regions in (a).

663

664



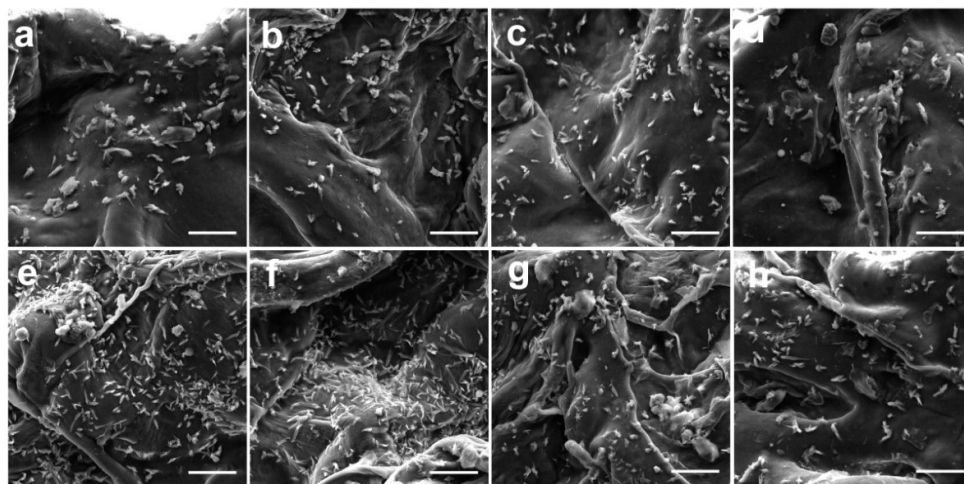
665

666 **Figure 4.** The photograph of RCS/G2 sponge after being immersed in PBS solution for 2 min (a),

667 the bar is 1 cm. Cumulative bFGF release from RCS and RCS/G2 sponges (b), and individual

668 points represent the mean values  $\pm$  standard deviation (SD) from three sponges samples.

669

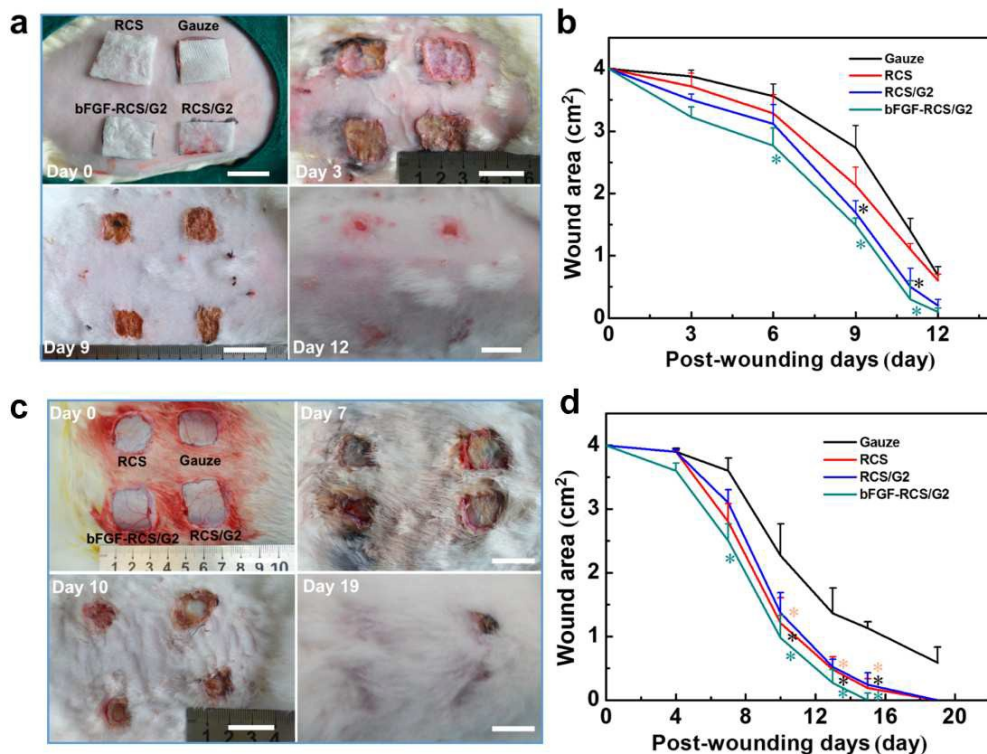


670

671 **Figure 5.** RCS (a, e), RCS/G2(b, f), RCS/G8(c, g) and RCS/G15(d, h) sponges seeded with  
672 fibroblasts for 3 days (a-d) and 14 days (e-h) of culture. The bar is 50 $\mu$ m.

673

674

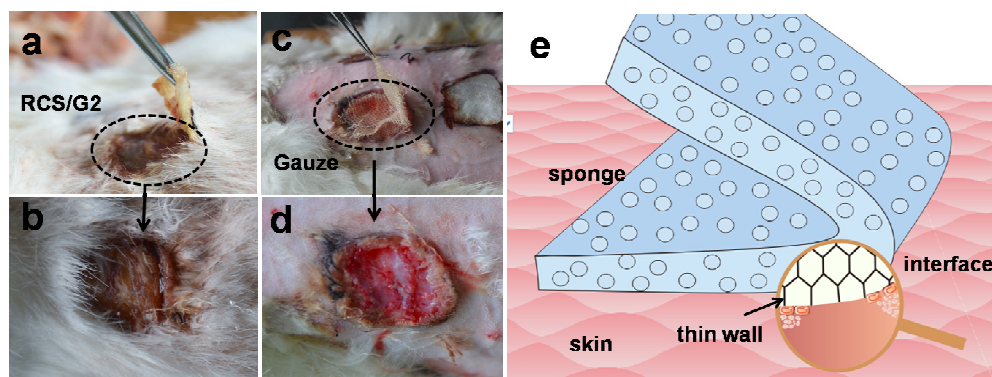


675

676 **Figure 6.** The wound closure of partial-thickness (a) and full-thickness (c) wounds treated with  
 677 gauze, RCS sponge, RCS/G2 sponge and bFGF-RCS/G2 sponge for days. The initial area of all  
 678 wounds on each rabbit was 4 cm<sup>2</sup>, and the bar is 2 cm. Evaluation of the partial-thickness (b) and  
 679 full-thickness wound area (d). The data represent the mean  $\pm$  SD of six rabbits. (\*  $P < 0.05$ ,  
 680 compared to control for same day).

681

682

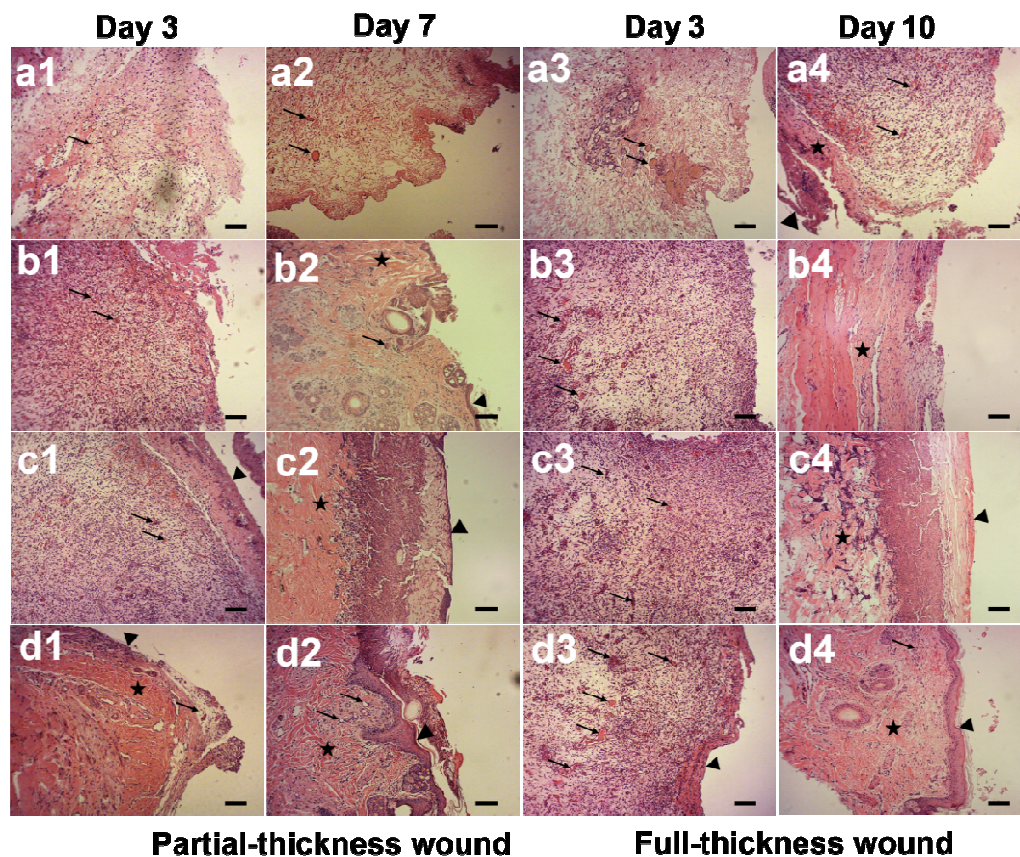


683

684 **Figure 7.** RCS/G2 sponge has easy-peeling property (a), preventing the secondary injury when  
685 removed from the wound (b); cotton gauze adheres to the wound surface when peeled (c), leading  
686 to the secondary injury (d); the schematic of interface between the sponge and the skin wound  
687 (e).

688

689

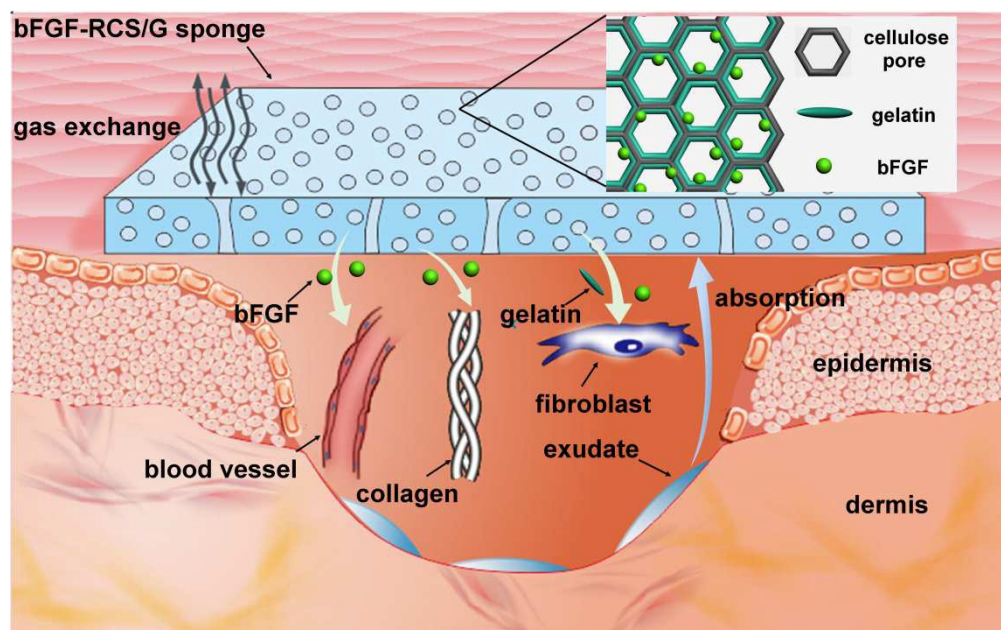


690

691 **Figure 8.** Histological images of skin tissues stained by hematoxylin and eosin (H&E) method  
 692 dissected in the post-operative day 3 (a1-d1) and day 7 (a2-d2) for partial-thickness wound, and in  
 693 day 3 (a3-d3) and day 10 (a4-d4) for full-thickness wound, respectively. The groups were RCS (b),  
 694 RCS/G2 (c), bFGF-RCS/G2 (d) sponges treated wound, and the medical cotton gauze (a) treated  
 695 wound was used as control. Scar bar is 100 $\mu$ m. The arrow, triangle and star represent blood vessel,  
 696 epidermis, collagen fibers, respectively.

697

698



699

700 **Figure 9.** The mechanism scheme to describe the promoting wound repair of bFGF-RCS/G  
701 sponges.

702

703

704 **Table 1.** The average nitrogen content ( $W_N$ , %), the average protein content ( $W_{Pro}$ , %), porosity  
 705 ( $P_r$ , %), water retention ratio ( $W_{wr}$ , %), the average pore size ( $d$ ,  $\mu\text{m}$ ) and swelling ratio ( $S$ , %) of  
 706 the RCS and RCS/G sponges.

Samples	$c$ (%)	$W_N$ (%)	$W_{Pro}$ (%)	$P_r$ (%)	$d$ ( $\mu\text{m}$ )	$W_{wr}$ (%)	$S$ (%)
RCS	0	0	0	97.3	97.0	717	1.00
RCS/G2	2	4.67	29.2	94.4	102	768	5.00
RCS/G8	8	5.61	35.1	85.7	110	774	8.60
RCS/G15	15	7.36	46.0	70.8	117	787	17.0
Gelatin	100	15.1	94.3	-	-	-	-
Gauze	-	-	-	-	-	110	-

707  $c$ : the concentration of gelatin solution .

708

709

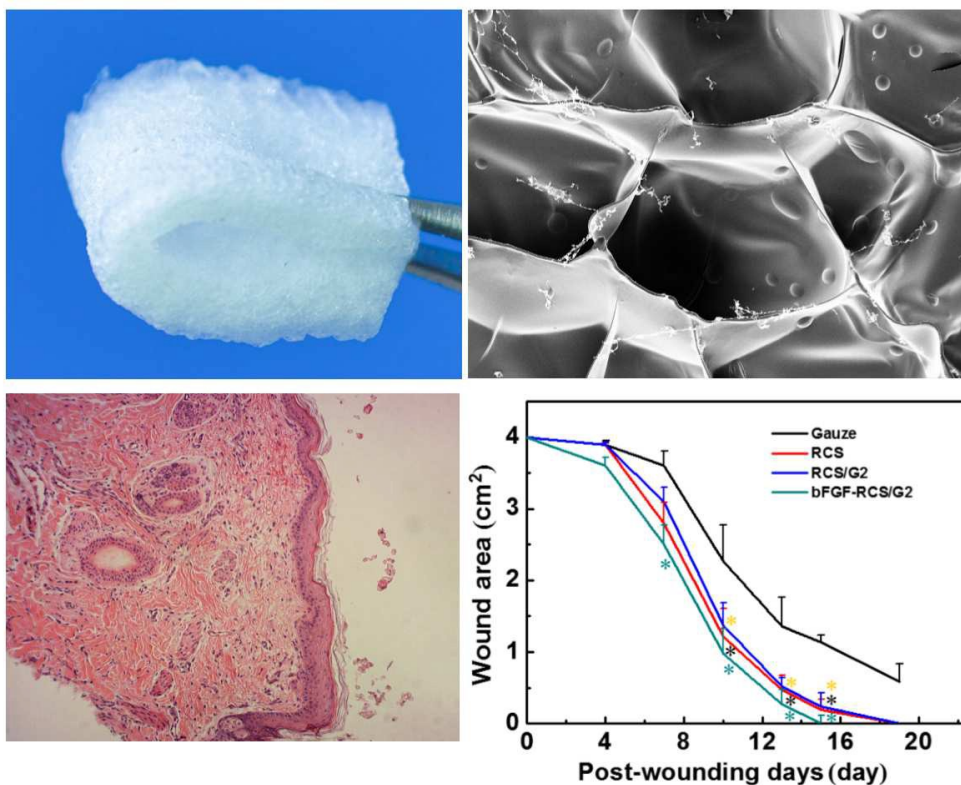
710 **Table 2.** The compressive moduli (kPa) and compressive strength (kPa) of RCS sponge, RCS/G  
711 sponges, and porous scaffolds or sponges derived from other natural polymers.

<b>Samples</b>	<b>Compressive moduli (kPa)</b>	<b>Compressive strength (kPa)</b>
<b>RCS</b>	<b>160±10</b>	<b>110±5</b>
<b>RCS/G2</b>	<b>490±12</b>	<b>266±7</b>
<b>RCS/G8</b>	<b>600±10</b>	<b>360±9</b>
<b>RCS/G15</b>	<b>750±16</b>	<b>400±10</b>
<b>Collagen<sup>[42]</sup></b>	<b>150</b>	<b>15</b>
<b>Collagen/Chitosan<sup>[42]</sup></b>	<b>500</b>	<b>30</b>
<b>Chitosan<sup>[42]</sup></b>	<b>750</b>	<b>45</b>
<b>Aginate<sup>[43, 44]</sup></b>	<b>230-1300</b>	<b>-</b>
<b>Silk<sup>[45]</sup></b>	<b>170-220</b>	<b>20-80</b>

712

713

## Table of content



The cellulose sponges loading gelatin and fibroblast growth factor as wound dressing were constructed directly from cellulose solution via a simple, green and cost-effective pathway. The cellulose sponges effectively promoted wound healing, as a result of the macro- and micro porous architecture.